

# Synthesis and characterization of Cu(I) isocyanide complexes exhibiting reversible luminescence

Takuya Hayakawa, Chika Nanzan, Masashi Hashimoto, Hiroyuki Teramae, and Tomomi Sakata\*

*Department of Chemistry, Faculty of Science, Josai University, Sakado, Saitama 350-0295, Japan*

\*E-mail: sakata@josai.ac.jp

Herein, we describe the synthesis of Cu(I) isocyanide complexes, namely, the [CuI(PDI)] (PDI = 1,4-phenylene diisocyanide) dimer and [Cu<sub>2</sub>I<sub>2</sub>(PPh<sub>3</sub>)<sub>2</sub>(PDI)<sub>2</sub>] (PPh<sub>3</sub> = triphenylphosphine), which exhibit weak orange (quantum yield  $\Phi = 1\%$ ) and intense pale blue ( $\Phi = 13\%$ ) emissions in the solid state under UV irradiation, respectively. Upon grinding, the luminescence of the [CuI(PDI)] dimer does not change, whereas that of [Cu<sub>2</sub>I<sub>2</sub>(PPh<sub>3</sub>)<sub>2</sub>(PDI)<sub>2</sub>] changes to a weak olive ( $\Phi = 4\%$ ) emission. Treatment of the ground [Cu<sub>2</sub>I<sub>2</sub>(PPh<sub>3</sub>)<sub>2</sub>(PDI)<sub>2</sub>] with an organic solvent and subsequent drying restore its original pale blue emission, which is indicative of reversible luminescent mechanochromism. Moreover, both the [CuI(PDI)] dimer and [Cu<sub>2</sub>I<sub>2</sub>(PPh<sub>3</sub>)<sub>2</sub>(PDI)<sub>2</sub>] exhibit thermochromism, i.e., their emissions change to a very intense green emission at 77 K. In particular, time-dependent density functional theory calculations reveal that [Cu<sub>2</sub>I<sub>2</sub>(PPh<sub>3</sub>)<sub>2</sub>(PDI)<sub>2</sub>] could be assigned to luminescence induced by halide-to-ligand charge transfer.

## 1. Introduction

The use of phosphorescent emissive  $d^6$  and  $d^8$  complexes [typically those of Ru(II), Ir(III), and Pt(II)] has significantly improved the performance of organic light-emitting diodes (OLEDs). Unfortunately, the above platinum-group elements are scarce, which requires the development of high-efficiency OLEDs based on luminescent complexes of other metals. In particular, luminescent  $d^{10}$  complexes have attracted increased attention because they do not feature d-d transitions and thus exhibit the advantage of greatly suppressed nonradiative deactivation.<sup>1,2)</sup> Another feature of luminescent  $d^{10}$  metal complexes is the wide variety of structures and available ligands, which benefits both material design and synthesis, as exemplified by the emissive  $d^{10}$  complexes of Au(I), Ag(I), and Cu(I) with ligands such as phosphines and pyridines.<sup>3)</sup> Recently, Cu(I) complexes have received increased attention because they are as strongly emissive as their Au(I) counterparts and are based on the relatively inexpensive and abundant Cu metal.<sup>4-10)</sup> Depending on the coligand(s), the high affinity of Cu(I) for halogen ligands affords a diverse group of complexes with mono-, di-, and tetranuclear discrete units, as well as halogen-bridged coordination oligomers and polymers. Among the Cu(I)-halide complexes, Cu(I)-iodide ones are well known for their structurally rich photophysical behavior and high luminescence efficiency.<sup>11-22)</sup> In this context, the modification of the luminescence color of these complexes in response to external mechanical stimuli and the subsequent reversion to the original luminescence color upon recrystallization is a subject of great interest. Although luminescent Cu(I)-iodide complexes containing ligands coordinated via pnictogen and chalcogen atoms have been extensively studied, complexes based on coordination via other elements are relatively underexplored. Herein, given the interesting luminescent properties of Au(I) isocyanide complexes,<sup>23-28)</sup> we focus on their Cu(I) analogs, which exhibit reversible mechanochromism (piezochromism).

## 2. Experimental methods

### 2.1 General procedures

All commercially available starting materials and solvents were used as received without any purification. All manipulations were conducted at room temperature. All emission spectra were recorded using a spectrofluorometer (JASCO FP-6200) with a long-pass filter (Opto Sigma SCF-50S-37L). Absolute photoluminescence (PL) quantum yield was measured with a spectrometer (Hamamatsu Photonics C9920-02). For the identification of the molecular structure of the obtained complexes, elemental, Fourier transform infrared

(FT-IR), and powder X-ray diffraction (PXRD) analyses were performed using CHN Corder (Yanako MT-6), FT-IR (JASCO FT/IR-4600), XRD (Rigaku RINT-2000) instruments, respectively. In this work, the precision of the crystal parameters analyzed by PXRD from the values of  $R_{wp}$  and  $S$  was low, but because there were no fatal alerts in checkCIF of International Union of Crystallography, we were able to qualitatively analyze the molecular configuration.

## 2.2 Synthesis and structure of [CuI(PDI)] dimer

A solution of 1,4-phenylene diisocyanide (PDI; 100 mg, 0.78 mmol) in acetonitrile (75 mL) was added to an acetonitrile (75 mL) solution of CuI (149 mg, 0.78 mmol) to afford a yellow suspension that was stirred for 48 h under nitrogen. The resulting precipitate was filtered and washed with acetonitrile to afford an insoluble yellow powder in 79% yield. Anal calcd (wt%) for  $C_8H_4Cu_1I_1N_2$ : C, 30.16; H, 1.27; N, 8.79. Found (wt%): C, 30.06; H, 1.41; N; 8.78. Figure 1 shows the FT-IR spectra of PDI with a peak at approximately  $2131\text{ cm}^{-1}$  (assigned to the  $C\equiv N$  stretching vibration) and the obtained complex with a peak at around  $2176\text{ cm}^{-1}$  newly observed in the spectrum of the latter indicating the formation of a Cu–CN bond.<sup>29,30</sup> Thus, the obtained complex was concluded to have the basic structure shown in Fig. 2, as supported by the results of PXRD analysis (Fig. 3 and Table I).<sup>31</sup> Moreover, the above PXRD pattern revealed that the obtained complex featured a head-to-tail configuration, with only one of the two isocyno groups of PDI coordinating to Cu. The Cu...Cu separation is equal to about  $2.60\text{ \AA}$ , showing that the obtained complex forms the dimer through the Cu...Cu interaction. Moreover, the adjacent benzene rings of PDIs in the dimer adopt a face-to-face geometry with a weak  $\pi$ - $\pi$  stacking interaction, whose minimum distance equals about  $3.30\text{ \AA}$ . This stacking contributes to realizing the greater stability of the dimeric structure. Figure 4 shows the relationship between reaction time and yield/(1 – yield), that is, the latter parameter was constant after stirring for 24 h, with the corresponding rate constant (determined from the slope of the above correlation at time < 24 h) estimated as  $37\text{ M}^{-1}\text{ h}^{-1}$ . Thus, on the basis of these results, a reaction time of 48 h was appropriate.

## 2.3 Synthesis and structure of [Cu<sub>2</sub>I<sub>2</sub>(PPh<sub>3</sub>)<sub>2</sub>(PDI)<sub>2</sub>]

A solution of CuI (223 mg, 1.17 mmol) and PPh<sub>3</sub> (307 mg, 1.17 mmol) in acetonitrile (150 mL) was added to an acetonitrile solution (50 mL) of PDI (150 mg, 1.17 mmol), which resulted in the formation of a white suspension. The suspension was stirred for 48 h under nitrogen and filtered, and the residue was washed with acetonitrile to afford

[Cu<sub>2</sub>I<sub>2</sub>(PPh<sub>3</sub>)<sub>2</sub>(PDI)<sub>2</sub>] as an insoluble white powder in 78% yield. Anal calcd (wt%) for C<sub>52</sub>H<sub>38</sub>Cu<sub>2</sub>I<sub>2</sub>N<sub>4</sub>P<sub>2</sub>: C, 53.76; H, 3.30; N, 4.82. Found (wt%): C, 54.14; H, 3.33; N, 4.90. The results of PXRD analysis supported the chemical structure shown in Fig. 5. Figure 6 and Table I respectively show the graphical representation and crystal parameters of [Cu<sub>2</sub>I<sub>2</sub>(PPh<sub>3</sub>)<sub>2</sub>(PDI)<sub>2</sub>].<sup>32)</sup> In the above structure, each Cu ion is bonded to one P atom of PPh<sub>3</sub> and one C atom of PDI; thus, the structure is fourfold-coordinated. The two Cu ions are bridged by two I<sup>-</sup> ligands to form a planar rhombic {Cu<sub>2</sub>I<sub>2</sub>} core with equal Cu–I distances {2.80(2), 2.809(17) Å} and unequal bond angles {Cu–I–Cu, 82.8(7)°, I–Cu–I, 97.2(7)°}, whereas the Cu...Cu separation equals 4.21 Å. The FT-IR spectra of the [CuI(PDI)] dimer (Fig. 1) and [Cu<sub>2</sub>I<sub>2</sub>(PPh<sub>3</sub>)<sub>2</sub>(PDI)<sub>2</sub>] (Fig. 7) show the C–H out-of-plane bending vibration of 1-substituted benzene at around 694 and 746 cm<sup>-1</sup> for [Cu<sub>2</sub>I<sub>2</sub>(PPh<sub>3</sub>)<sub>2</sub>(PDI)<sub>2</sub>], which supports the chemical structure of this complex shown in Fig. 5. Similarly to the case of the dimer of [CuI(PDI)], the relationship between reaction time and yield/(1 – yield) was also examined (Fig. 8), with the latter parameter being constant after stirring for 8 h. On the basis of the slope of the above correlation (time < 8 h), the corresponding rate constant was estimated as 103 M<sup>-1</sup> h<sup>-1</sup>, which is almost threefold higher than that obtained for the dimer of [CuI(PDI)], thus revealing that the introduction of an electron-donating PPh<sub>3</sub> group markedly increases the reaction rate. On the basis of these data, 48 h as the reaction time was concluded to be sufficient.

### 3. Results and discussion

#### 3.1 Thermochromism

The dimer of [CuI(PDI)] exhibited a weak orange emission under UV irradiation (excitation and emission spectra were measured at 295 K, and the excitation wavelength of the excitation spectrum was fixed to 350 nm). As shown in Fig. 9, the excitation spectrum of the dimer of [CuI(PDI)] featured two peaks at 329 and 360 nm, which originated from the π-π\* transitions of PDI. Conversely, four peaks (411, 470, 519, and 611 nm) were observed in the emission spectrum, implying the existence of four distinct transitions. Moreover, the emission spectrum measured at 77 K featured a strong peak at 528 nm.

On the other hand, [Cu<sub>2</sub>I<sub>2</sub>(PPh<sub>3</sub>)<sub>2</sub>(PDI)<sub>2</sub>] exhibited a pale blue emission under UV irradiation; its excitation and emission spectra are shown in Fig. 10. Two peaks (330 and 370 nm) and one peak (352 nm) were observed in the excitation spectrum, which are ascribed to the π-π\* transitions of PDI and PPh<sub>3</sub>. A broad peak with λ<sub>max</sub> = 474 nm was observed in the emission spectrum, which corresponds to one distinct transition. The luminescence quantum

yield was determined as 13%, which is 13 times higher than that of the dimer of [CuI(PDI)], which was attributed to the different core structure of these complexes. That is, the halogen (iodide in this work)-bridged coordination suppresses the rotation and vibration of the halogen terminal in the dinuclear halide complex, whereas the halogen in the mononuclear halide complex can rotate and vibrate freely, which leads to the promotion of inradiative deactivation resulting in the decrease in quantum yield. Moreover, the emission spectrum recorded at a lower temperature showed gradual peak shifts to a longer wavelength and a higher peak intensity, which is the feature of excimer emission.<sup>33)</sup> Here, the temperature dependence on  $\lambda_{\max}$  was examined in more detail to investigate the emission mechanism. As shown in Fig. 11, above 215 K, the inverse of  $\lambda_{\max}$  linearly decreased with the reciprocal of temperature, and below 215 K, it remained constant regardless of the reciprocal of temperature, i.e.,  $\lambda_{\max} = 500$  nm. This means that there are two (temperature-dependent and temperature-independent) emission regions in a single complex. The former was predominantly derived from the excimer based on the dipole-dipole interaction (Keesom force), which is expected to be fluorescent from the viewpoint of conventional excimer lifetime, whereas the latter, which is expected to be phosphorescent, was the emission regardless of the following equation of Keesom energy:<sup>34,35)</sup>

$$U(r) = - \frac{1}{3kT} \left( \frac{\mu_1 \mu_2}{4\pi \epsilon_0 \epsilon_r} \right)^2 \frac{1}{r^6}. \quad (1)$$

Here,  $\mu_1$  and  $\mu_2$  are the dipole moments in the ground and excited states of complexes, respectively,  $\epsilon_0$  is the permittivity of free space,  $\epsilon_r$  is the dielectric constant of the surrounding material, T is the absolute temperature, k is the Boltzmann constant, and r is the distance between dipoles.  $\mu_1$  and  $\mu_2$  are solved using density functional theory (DFT) and time-dependent density functional theory (TD-DFT) calculations using Gaussian09 software and the B3PW91 density functional in this work. 6-31G(d,p) was used as a basis set for H, C, N, P, and Cu, whereas lanl2dz was used for I.<sup>36-38)</sup> From the slope above 215 K in Fig. 11 and Eq. (1), the distance between dipoles was estimated to be around 2.5 Å, which is found to be valid in comparison with that of the conventional dipole-dipole interaction ( $\sim 3$  Å).<sup>39)</sup> In addition, the small difference between the wavelengths of emission peaks observed below 215 K indicated that the change in the structure of excited states was almost insensitive to temperature.

Furthermore, the luminescence property of [Cu<sub>2</sub>I<sub>2</sub>(PPh<sub>3</sub>)<sub>2</sub>(PDI)<sub>2</sub>] was examined by TD-

DFT calculations, where the configuration of  $[\text{Cu}_2\text{I}_2(\text{PPh}_3)_2(\text{PDI})_2]$  was treated as not an excimer but an isolated molecule.<sup>40)</sup> TD-DFT calculations accompanied by structure optimization were carried out using the molecular structure that was optimized by DFT calculation as the initial one (see supplementary data). The oscillator strengths and excited state energies in absorption (vertical excitation) processes, which are solved by TD-DFT calculations in this work, are roughly treated similarly to those in emission processes. Figure 12 and Table II show that the luminescence from the excited states 1, 2, and 3 was almost forbidden owing to the markedly small oscillator strength, and that HOMO-2 was localized on I, whereas the LUMO (almost  $\pi^*$ ) was localized on PDI, that is, luminescence from the excited state 4 is expected to correspond to XLCT. The calculated emission peak wavelength of 502 nm was close to the experimental value of 500 nm obtained below 215 K, meaning that the density functional and basis set we used in this work were appropriate. Moreover, this calculation results support the idea that the large difference in quantum yield between the  $[\text{CuI}(\text{PDI})]$  dimer and  $[\text{Cu}_2\text{I}_2(\text{PPh}_3)_2(\text{PDI})_2]$  (1 vs 13%) is derived from the differences in the degrees of rotation and vibration in the halogen terminal, which becomes the electron supplier for XLCT, as already above.

### 3.2 Luminescent mechanochromism

When solid  $[\text{Cu}_2\text{I}_2(\text{PPh}_3)_2(\text{PDI})_2]$  was ground with a pestle, it changed from white to yellow under ambient light, and a new weak emission ( $\lambda_{\text{max}} = 531 \text{ nm}$ ,  $\Phi = 4\%$ ) was observed (Fig. 13, dashed line). This olive emission reverted to the original pale blue one immediately after treating the ground powder with several drops of acetonitrile (dotted line). It was thus speculated that mechanical stimulation and treatment with an organic solvent resulted in the change and restoration of the molecular morphology. To confirm this speculation, the structural transformation of this complex was examined by PXRD. As shown in Fig. 14, the PXRD pattern of the unground complex shows numerous clear and intense reflection peaks, indicative of its crystalline nature. In contrast, these sharp peaks vanished after grinding, which implied the occurrence of a crystal-to-amorphous phase conversion. Moreover, Fig. 11 indicates that the inverse of  $\lambda_{\text{max}}$  for the ground powder remained constant ( $\lambda_{\text{max}} = 531 \text{ nm}$ ) regardless of the reciprocal temperature, and that the energy gap of the plateau region between the ground and unground powders was  $14.0 \text{ kJ mol}^{-1}$ , which is comparable to the energy of the change in crystal phases. Therefore, this red-shift phenomenon might be related to packing-dependent emission.<sup>41)</sup> For the unground complex, the adjacent molecules exhibited stronger intermolecular interactions with each other, which could help to further rigidify the

molecular conformation and block the nonradiative pathways, thus resulting in the relatively bluer emission and higher quantum yield (13%). For the amorphous powder, the poor molecular arrangement provided a large space for the intramolecular rotation and vibration, for example, owing to the decrease in bond energy or the incomplete dissociation of Cu-I bonds forming a planar rhombic  $\{\text{Cu}_2\text{I}_2\}$  core. These motions, such as those in the mononuclear complex, result in a much lower emission efficiency (4%).

Treatment with toluene or acetonitrile and their subsequent evaporation resulted in the reappearance of the intense and sharp reflection peaks, suggesting that the crystalline phase state was restored by the lattice repacking, where the intermolecular arrangement was modified from the thermodynamically unstable amorphous phase to the thermodynamically stable crystal phase by dropping an organic solvent. Therefore, the results of PXRD analysis indicated that the observed mechanochromism originated from a morphological transition between the crystalline and amorphous states. Notably, the above pale blue to olive emission change could be repeated without any decomposition, as confirmed by the reversible behavior of the PXRD peak intensity monitored at a diffraction angle of  $21.04^\circ$  (Fig. 15).

## 4. Conclusions

Herein, we successfully prepared the  $[\text{CuI}(\text{PDI})]$  dimer and  $[\text{Cu}_2\text{I}_2(\text{PPh}_3)_2(\text{PDI})_2]$  as yellow and white powders exhibiting weak orange and pale blue emissions under UV irradiation, respectively. For the  $[\text{CuI}(\text{PDI})]$  dimer, the luminescence quantum yield was experimentally determined as 1%. In contrast, the emission spectrum of  $[\text{Cu}_2\text{I}_2(\text{PPh}_3)_2(\text{PDI})_2]$  featured one intense broad peak predicted to be due to XLCT, with the corresponding luminescence quantum yield of 13%. However, we found a temperature-dependent emission (fluorescence) above 215 K, which was predominantly derived from the excimer on the basis of the dipole-dipole interaction (Keesom force), and a temperature-independent emission (phosphorescence) below 215 K. Both the  $[\text{CuI}(\text{PDI})]$  dimer and  $[\text{Cu}_2\text{I}_2(\text{PPh}_3)_2(\text{PDI})_2]$  exhibited emission thermochromism, but only  $[\text{Cu}_2\text{I}_2(\text{PPh}_3)_2(\text{PDI})_2]$ , being a dinuclear complex, exhibited luminescent mechanochromism. Moreover, mechanical grinding of  $[\text{Cu}_2\text{I}_2(\text{PPh}_3)_2(\text{PDI})_2]$  triggered a change in luminescence color observed under UV irradiation. Subsequent treatment with toluene or acetonitrile completely restored the color. This reversible change in color could be repeated multiple times.

## Acknowledgments

The authors thank Mr. Yusuke Yabara and Dr. Hiroshi Miyamae of Saitama University and Josai University for encouragement throughout this study. They are also grateful to Dr.

Mitsuaki Suzuki of Tokyo Gakugei University for valuable discussions.

## References

- 1) T. Tsubomura, T. Tsukuda, and K. Matsumoto, *Bull. Jpn. Soc. Coord. Chem.* **52**, 29 (2008) [in Japanese].
- 2) V. W.-W. Yam, V. K.-M. Au, and S.Y.-L. Leung, *Chem. Rev.* **115**, 7589 (2015).
- 3) K. Tsuge, *Chem. Lett.* **42**, 204 (2013).

- 4) P. C. Ford, E. Cariati, and J. Bourassa, *Chem. Rev.* **99**, 3625 (1999).
- 5) N. Armaroli, *Chem. Soc. Rev.* **30**, 113 (2001).
- 6) R. C. Evans, P. Douglas, and C. J. Winscom, *Coord. Chem. Rev.* **250**, 2093 (2006).
- 7) A. L.-Cambot, M. Cantuel, Y. Leydet, G. Jonusauskas, D. M. Bassani, and N. D. McClenaghan, *Coord. Chem. Rev.* **252**, 2572 (2008).
- 8) A. Barbieri, G. Accorsi, and N. Armaroli, *Chem. Commun.*, 2185 (2008).
- 9) K. J. Lotito and J. C. Peters, *Chem. Commun.* **46**, 3690 (2010).
- 10) S.-P. Luo, E. Mejia, A. Friedrich, A. Pazidis, H. Junge, A.-E. Surkus, R. Jackstell, S. Denurra, S. Gladiali, S. Lochbrunner, and M. Beller, *Angew. Chem., Int. Ed.* **52**, 419 (2013).
- 11) K. R. Kyle, C. K. Ryu, J. A. DiBenedetto, and P. C. Ford, *J. Am. Chem. Soc.* **113**, 2954 (1991).
- 12) E. Cariati, J. Bourassa, and P. C. Ford, *Chem. Commun.*, 1623 (1998).
- 13) T. Tsubomura, S. Enoto, S. Endo, T. Tamane, K. Matsumoto, and T. Tsukuda, *Inorg. Chem.* **44**, 6373 (2005).
- 14) S. Lee, S. Park, Y. Kang, S.-H. Moon, S. S. Lee, and K.-M. Park, *Bull. Korean Chem. Soc.* **29**, 1811 (2008).
- 15) S. Perruchas, X. F. Le Goff, S. Maron, I. Maurin, F. Guillen, A. Garcia, T. Gacoin, and J.-P. Boilot, *J. Am. Chem. Soc.* **132**, 10967 (2010).
- 16) M. Hashimoto, S. Igawa, M. Yashima, I. Kawata, M. Hoshino, and M. Osawa, *J. Am. Chem. Soc.* **133**, 10348 (2011).
- 17) Z. Liu, M. F. Qayyum, C. Wu, M. T. Whited, P. I. Djurovich, K. O. Hodgson, B. Hedman, E. I. Solomon, and M. E. Thompson, *J. Am. Chem. Soc.* **133**, 3700 (2011).
- 18) L. Maini, D. Braga, P. P. Mazzeo, and B. Ventura, *Dalton Trans.* **41**, 531 (2012).
- 19) T. Hayashi, A. Kobayashi, H. Ohara, M. Yoshida, T. Matsumoto, H.-C. Chang, and M. Kato, *Inorg. Chem.* **54**, 8905 (2015).
- 20) A. Kobayashi, T. Hasegawa, M. Yoshida, and M. Kato, *Inorg. Chem.* **55**, 1978 (2016).
- 21) K. Tsuge, Y. Chishina, H. Hashiguchi, Y. Sasaki, M. Kato, S. Ishizawa, and N. Kitamura, *Coord. Chem. Rev.* **306**, 636 (2016).
- 22) J. Nishida, H. Ohura, Y. Kita, H. Hasegawa, T. Kawase, N. Takada, H. Sato, Y. Sei, and Y. Yamashita, *J. Org. Chem.* **81**, 433 (2016).
- 23) K. Kawaguchi, T. Seki, T. Karatsu, A. Kitamura, H. Ito, and S. Yagai, *Chem. Commun.* **49**, 11391 (2013).
- 24) T. Seki, K. Sakurada, and H. Ito, *Chem. Commun.* **51**, 13933 (2015).
- 25) M. Jin, T. Seki, and H. Ito, *Chem. Commun.* **52**, 8083 (2016).

- 26) T. Seki, M. Jin, and H. Ito, *Inorg. Chem.* **55**, 12309 (2016).
- 27) K. Sakurada, T. Seki, and H. Ito, *CrystEngComm* **18**, 7217 (2016).
- 28) T. Seki, K. Kobayashi, and H. Ito, *Chem. Commun.* **53**, 6700 (2017).
- 29) G. A. Bowmaker, B. J. Kennedy, and J. C. Reid, *Inorg. Chem.* **37**, 3968 (1998).
- 30) J. Díez, M. P. Gamasa, J. Gimeno, M. Lanfranchi, and A. Tiripicchio, *J. Organomet. Chem.* **3**, 677 (2001).
- 31) Crystal data for dimer of [CuI(PDI)] CCDC-1567184.
- 32) Crystal data for [Cu<sub>2</sub>I<sub>2</sub>(PPh<sub>3</sub>)<sub>2</sub>(PDI)<sub>2</sub>] CCDC-1567192.
- 33) O. Khorev, C. D. Bösch, M. Probst, and R. Häner, *Chem. Sci.* **5**, 1506 (2014).
- 34) R. H. French, *J. Am Ceram. Soc.* **83**, 2117 (2000).
- 35) J. N. Israelachvili, *Intermolecular and Surface Forces* (Academic Press, New York, 1992) Chap. 2, p. 34.
- 36) P. J. Hay and W. R. Wadt, *J. Chem. Phys.* **82**, 270 (1985).
- 37) W. R. Wadt and P. J. Hay, *J. Chem. Phys.* **82**, 284 (1985).
- 38) P. J. Hay and W. R. Wadt, *J. Chem. Phys.* **82**, 299 (1985).
- 39) J. N. Israelachvili, *Intermolecular and Surface Forces* (Academic Press, New York, 1992) Chap. 4, p. 81.
- 40) F. D. Angelis, S. Fantacci, A. Sgamellotti, E. Cariati, R. Ugo, and P. C. Ford, *Inorg. Chem.* **45**, 10576 (2006).
- 41) C. Wang and Z. Li, *Mater. Chem. Front.* **1**, 2174 (2017).

## Figure captions

**Fig. 1. (Color online)** FT-IR spectra of (a) dimer of [CuI(PDI)] and (b) PDI.

**Fig. 2. (Color online)** Basic structure of [CuI(PDI)].

**Fig. 3. (Color online)** Partial view of crystal packing of dimer of [CuI(PDI)].

**Fig. 4. (Color online)** Relationship between reaction time and yield/(1 – yield) for dimer of [CuI(PDI)].

**Fig. 5. (Color online)** Chemical structure of  $[\text{Cu}_2\text{I}_2(\text{PPh}_3)_2(\text{PDI})_2]$ .

**Fig. 6. (Color online)** Partial view of crystal packing in  $[\text{Cu}_2\text{I}_2(\text{PPh}_3)_2(\text{PDI})_2]$ .

**Fig. 7. (Color online)** FT-IR spectra of (a) dimer of  $[\text{CuI}(\text{PDI})]$  and (b)  $[\text{Cu}_2\text{I}_2(\text{PPh}_3)_2(\text{PDI})_2]$ .

**Fig. 8. (Color online)** Relationship between reaction time and yield/(1 – yield) for  $[\text{Cu}_2\text{I}_2(\text{PPh}_3)_2(\text{PDI})_2]$ .

**Fig. 9. (Color online)** Emission and excitation spectra of dimer of  $[\text{CuI}(\text{PDI})]$  at 77 and 295 K.

**Fig. 10. (Color online)** Emission and excitation spectra of  $[\text{Cu}_2\text{I}_2(\text{PPh}_3)_2(\text{PDI})_2]$  at 77 and 295 K.

**Fig. 11. (Color online)** Relationship between the inverse of  $\lambda_{\text{max}}$  and the reciprocal of temperature (a) before and (b) after grinding.

**Fig. 12. (Color online)** Schematic molecular orbital diagrams and orbital shapes related to the calculated transitions of  $[\text{Cu}_2\text{I}_2(\text{PPh}_3)_2(\text{PDI})_2]$ .

**Fig. 13. (Color online)** Emission spectra of  $[\text{Cu}_2\text{I}_2(\text{PPh}_3)_2(\text{PDI})_2]$  before and after grinding and after subsequent treatment with  $\text{CH}_3\text{CN}$ .

**Fig. 14. (Color online)** PXRD patterns of  $[\text{Cu}_2\text{I}_2(\text{PPh}_3)_2(\text{PDI})_2]$  (a) before grinding, (b) after grinding, (c) first treatment with toluene, (d) second grinding, (e) second treatment, (f) third grinding, and (g) third treatment.

**Fig. 15. (Color online)** Intensity of the  $[\text{Cu}_2\text{I}_2(\text{PPh}_3)_2(\text{PDI})_2]$  PXRD peak at  $21.04^\circ$ .

**Table I.** Crystal parameters of dimer of [CuI(PDI)] and [Cu<sub>2</sub>I<sub>2</sub>(PPh<sub>3</sub>)<sub>2</sub>(PDI)<sub>2</sub>].

Formula	Dimer of [CuI(PDI)]	[Cu <sub>2</sub> I <sub>2</sub> (PPh <sub>3</sub> ) <sub>2</sub> (PDI) <sub>2</sub> ]
Crystal system, space group	Monoclinic, P2 <sub>1</sub> /c	Triclinic, P-1
<i>a, b, c</i> (Å)	9.285(4), 18.160(5), 6.810(2)	9.420(4), 9.748(4), 12.371(5)
<i>α, β, γ</i> (deg)	90, 103.83(3), 90	108.97(2), 106.128(16), 91.745(19)
<i>V</i> (Å <sup>3</sup> )	1115.0(7)	1022.9(7)
Density (g/cm <sup>3</sup> )	1.900	1.886
<i>Z</i>	4	1
<i>R</i> <sub>wp</sub>	0.2788	0.1349
<i>S</i>	5.9932	3.3283

**Table II.** Energy, oscillator strength, and major contributions of calculated transitions for [Cu<sub>2</sub>I<sub>2</sub>(PPh<sub>3</sub>)<sub>2</sub>(PDI)<sub>2</sub>].

Excited state	Energy (nm)	Oscillator strength	Major contribution (%)
1	935.11	0.0004	HOMO → LUMO (98)
2	642.71	0.0027	HOMO → LUMO+1 (99)
3	548.75	0.0005	HOMO-5 → LUMO (3) HOMO-2 → LUMO (10) HOMO-1 → LUMO (82)
<b>4</b>	<b>501.50</b>	<b>0.0606</b>	HOMO-7 → LUMO (3) <b>HOMO-2 → LUMO (80)</b> HOMO-1 → LUMO (10)

**Figures**

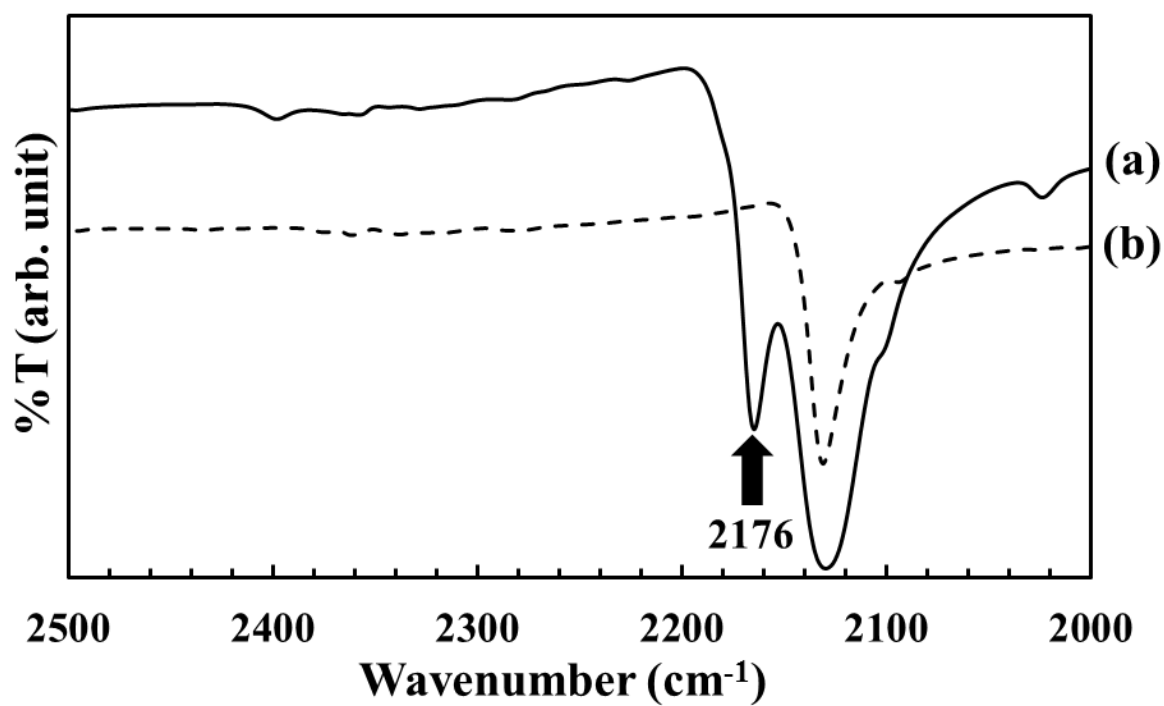


Fig. 1



Fig. 2



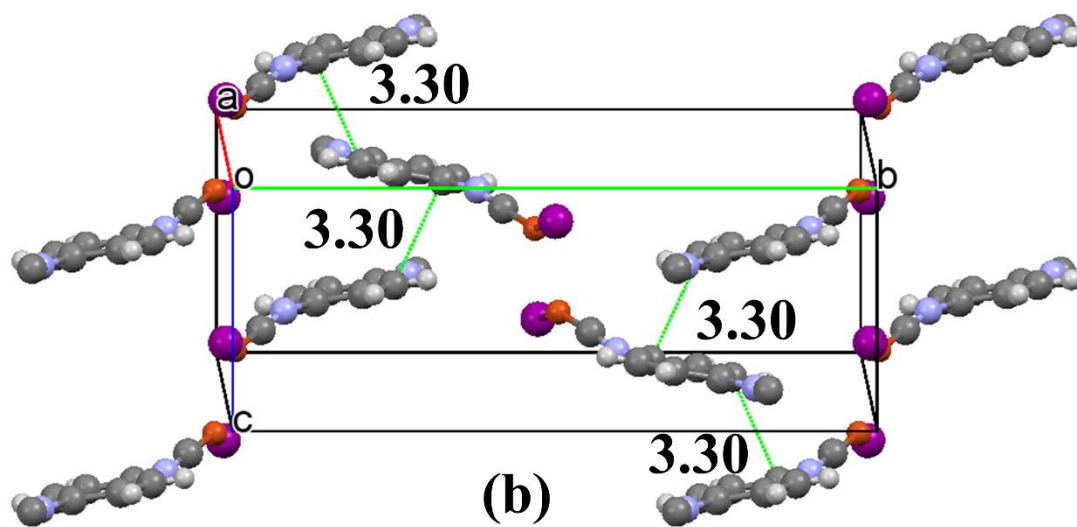
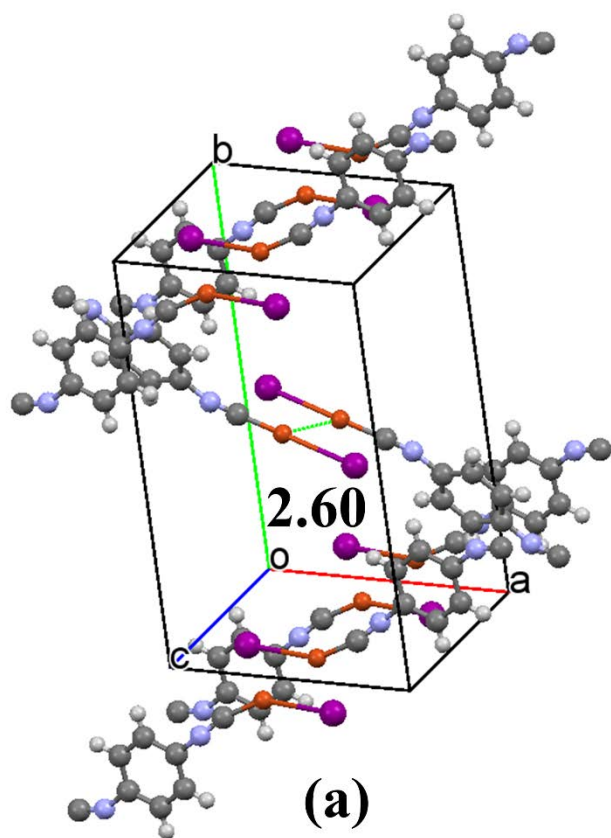


Fig. 3

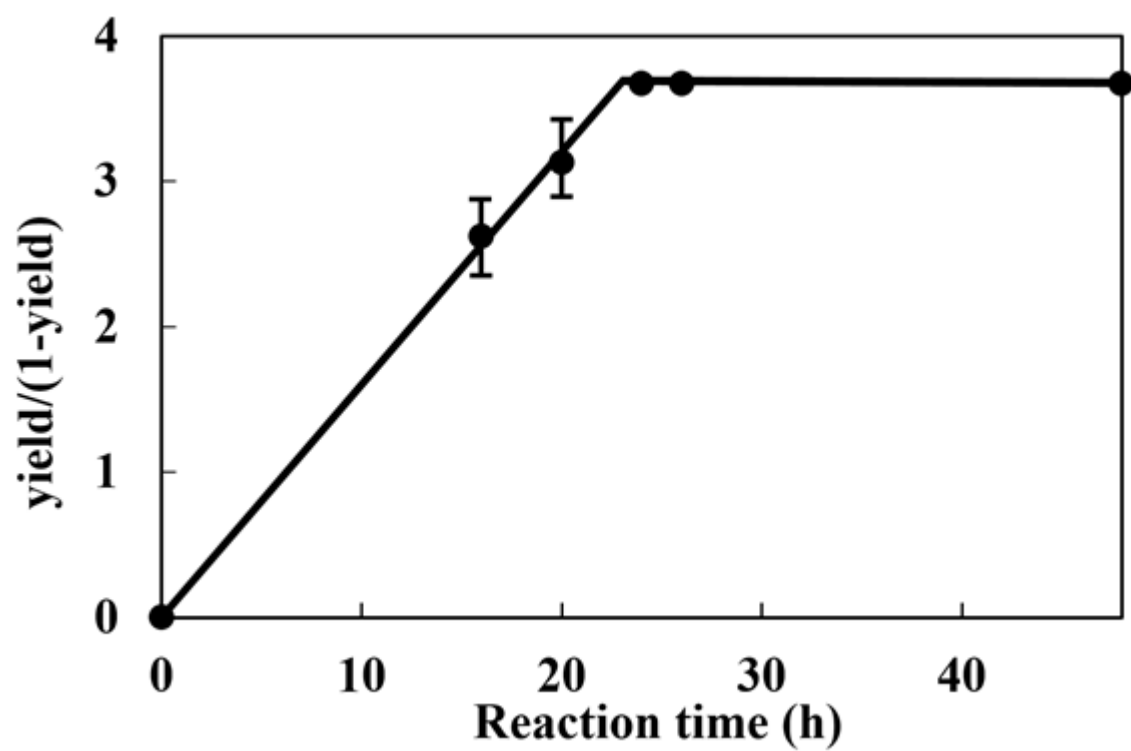


Fig. 4

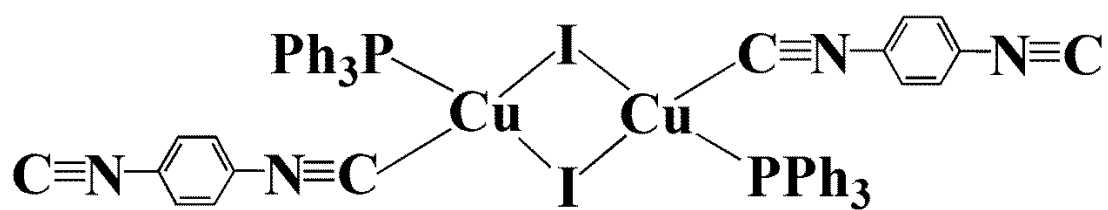


Fig. 5

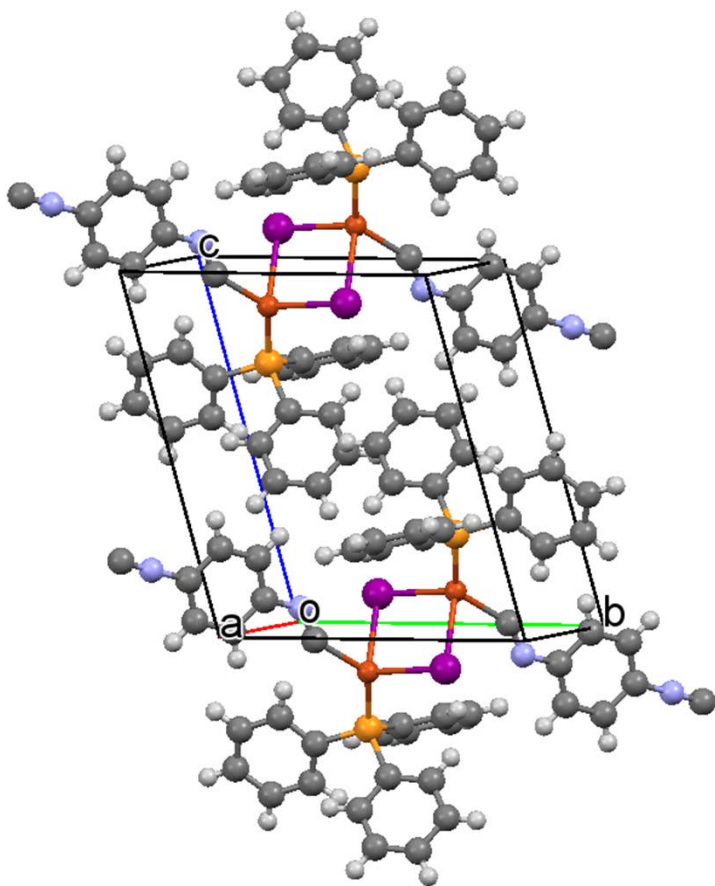


Fig. 6

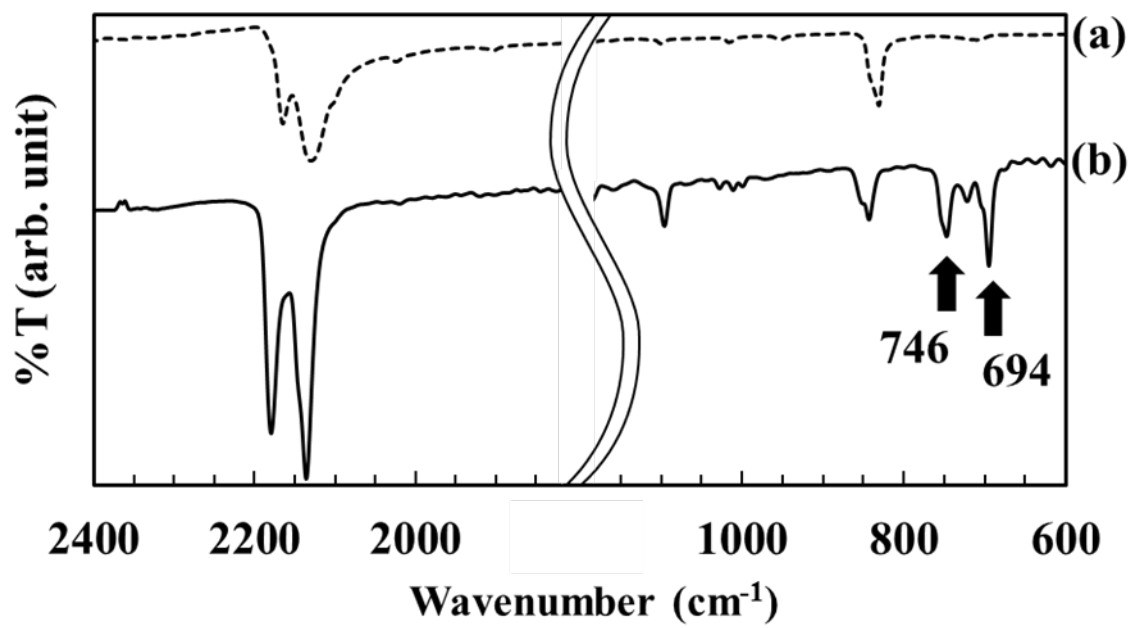


Fig. 7

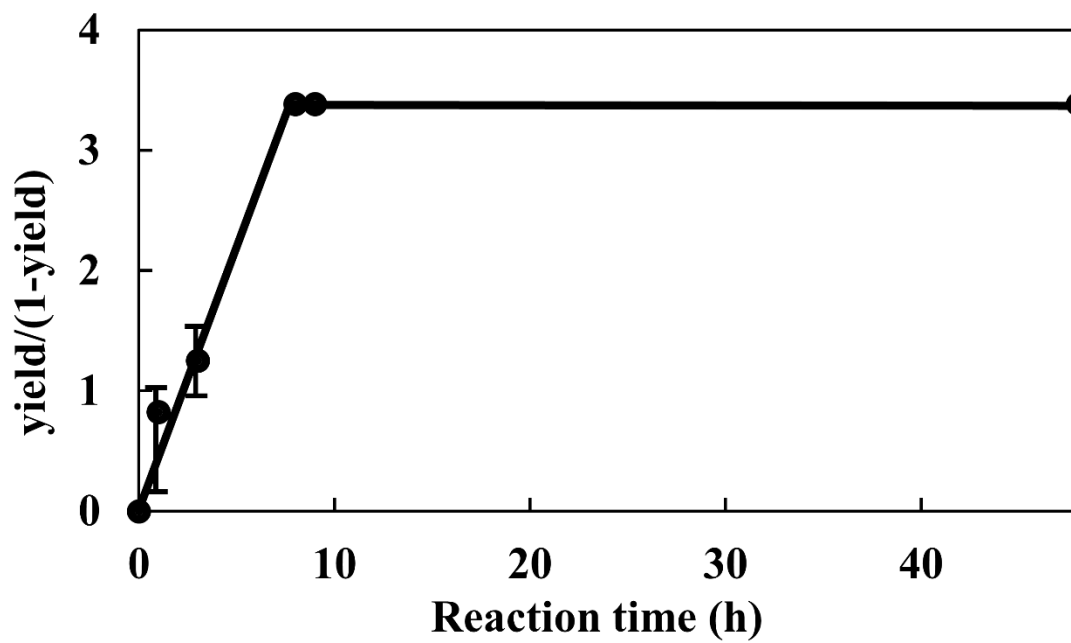


Fig. 8

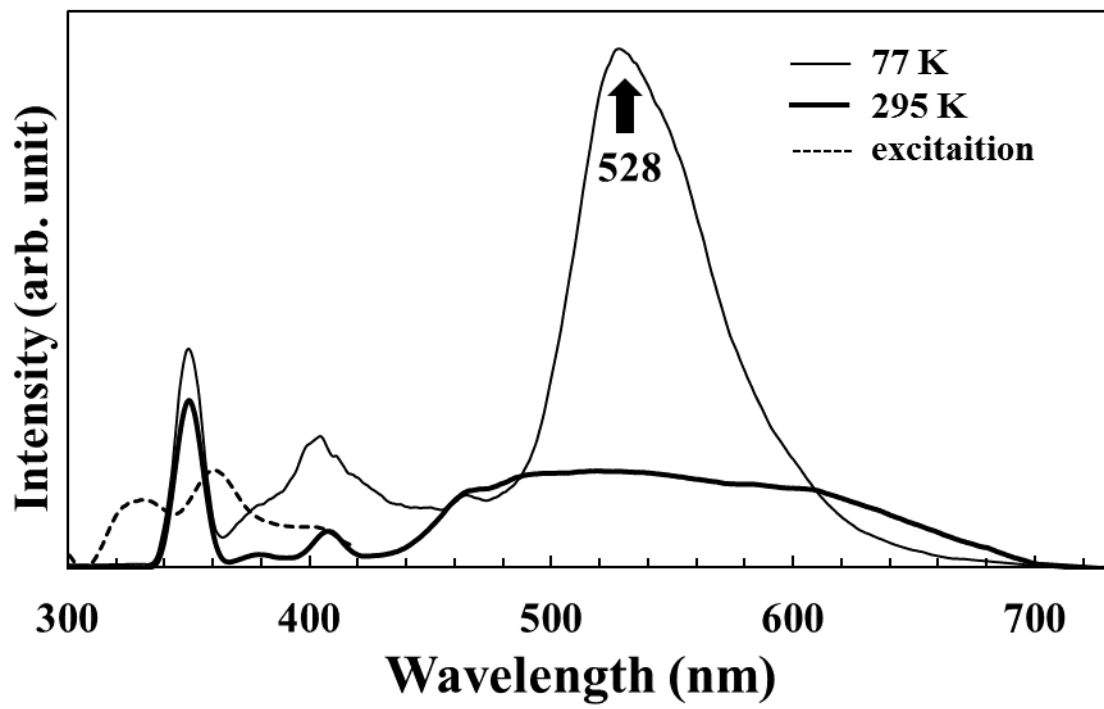


Fig. 9

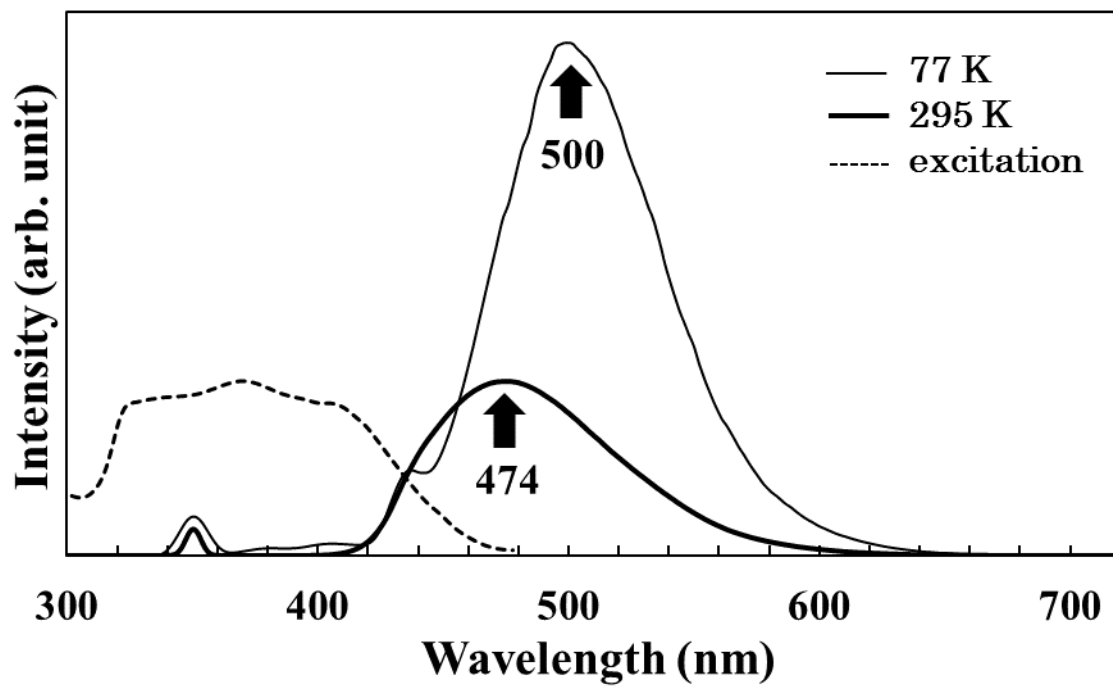


Fig. 10

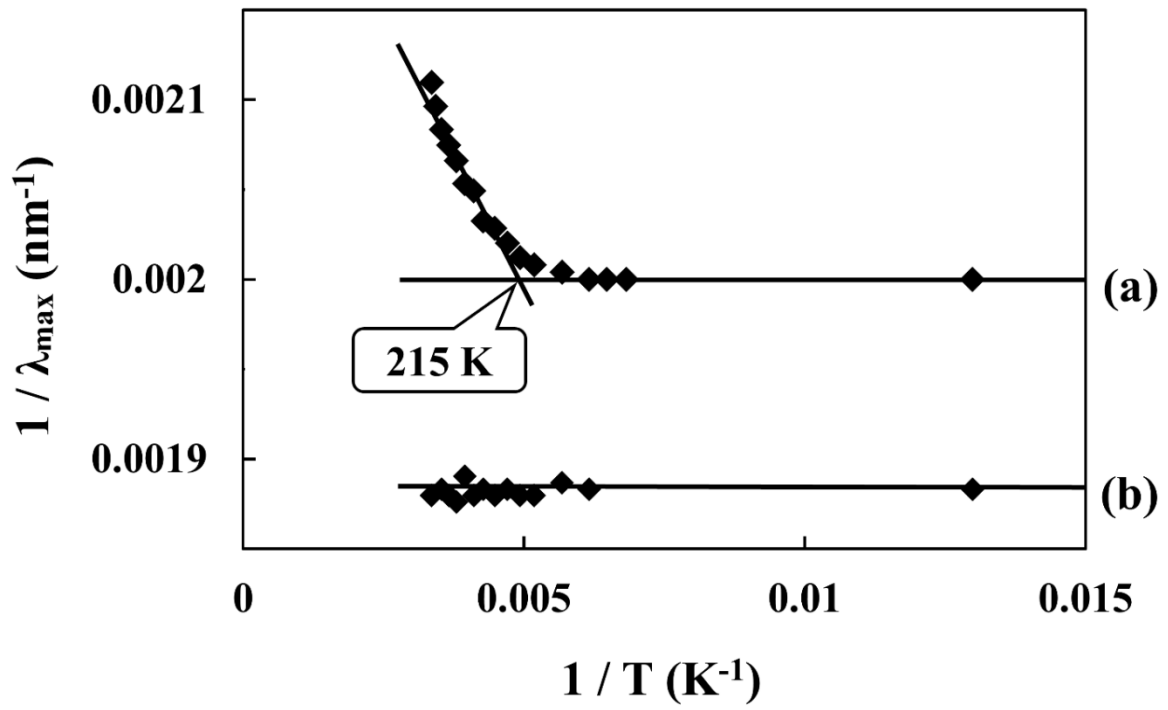


Fig. 11

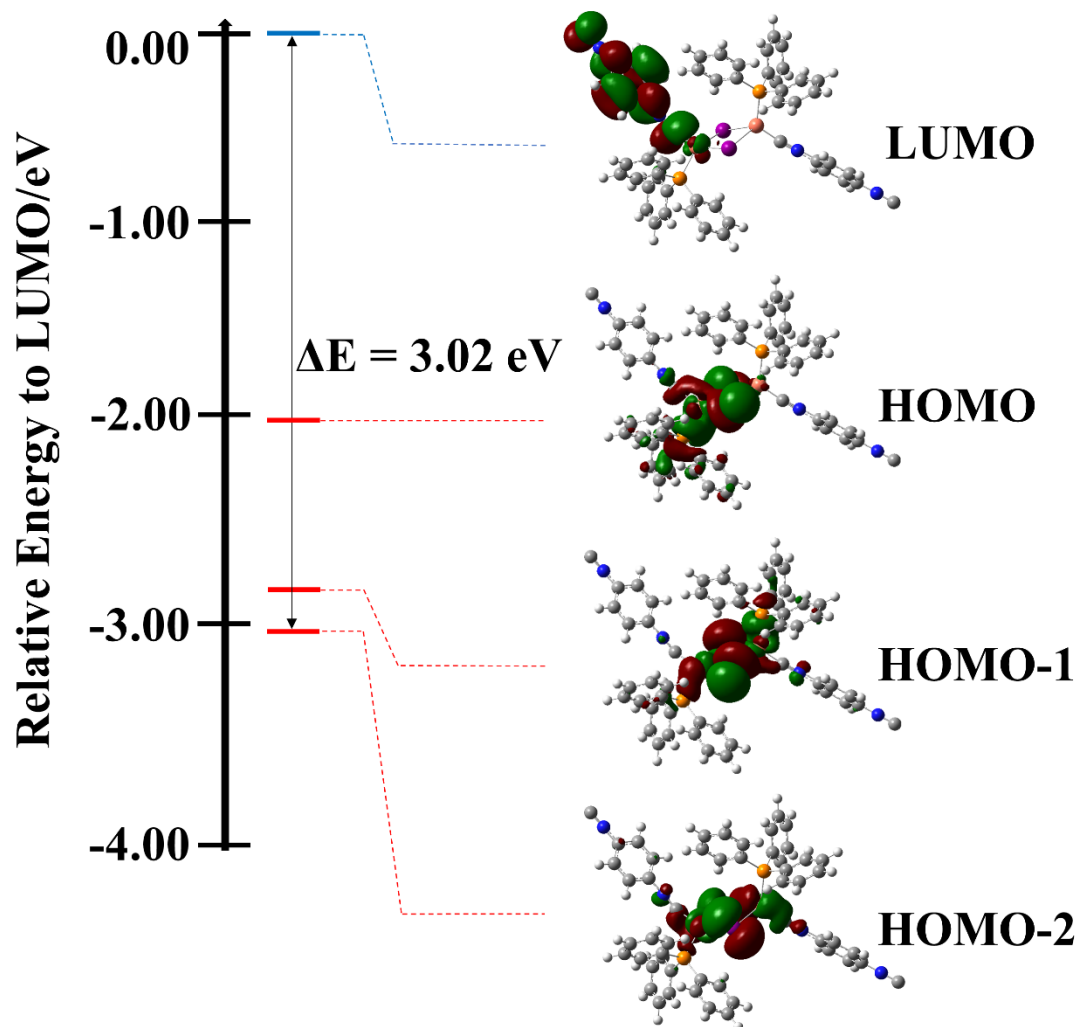


Fig. 12

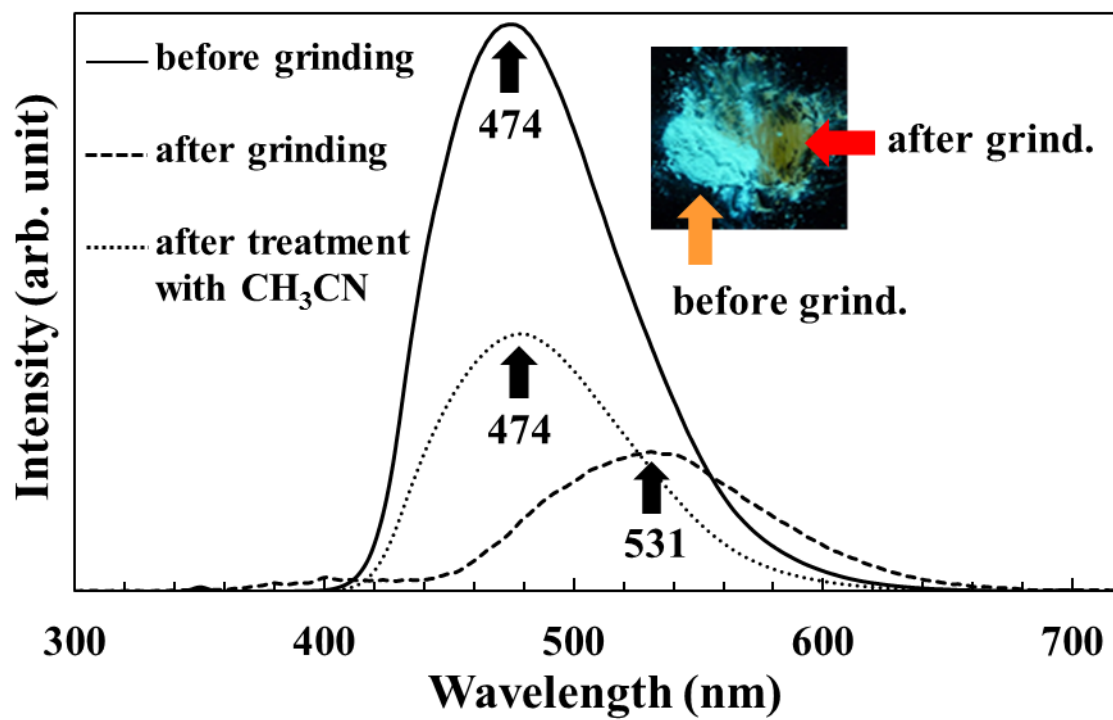


Fig. 13

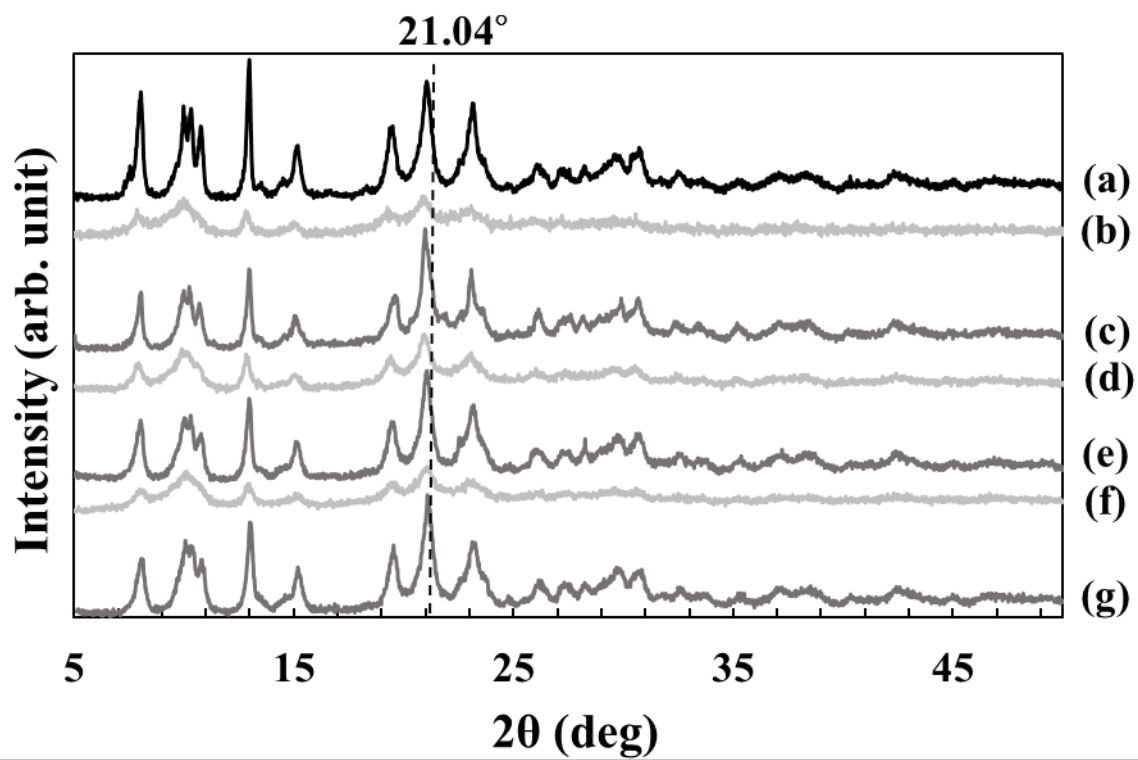


Fig. 14

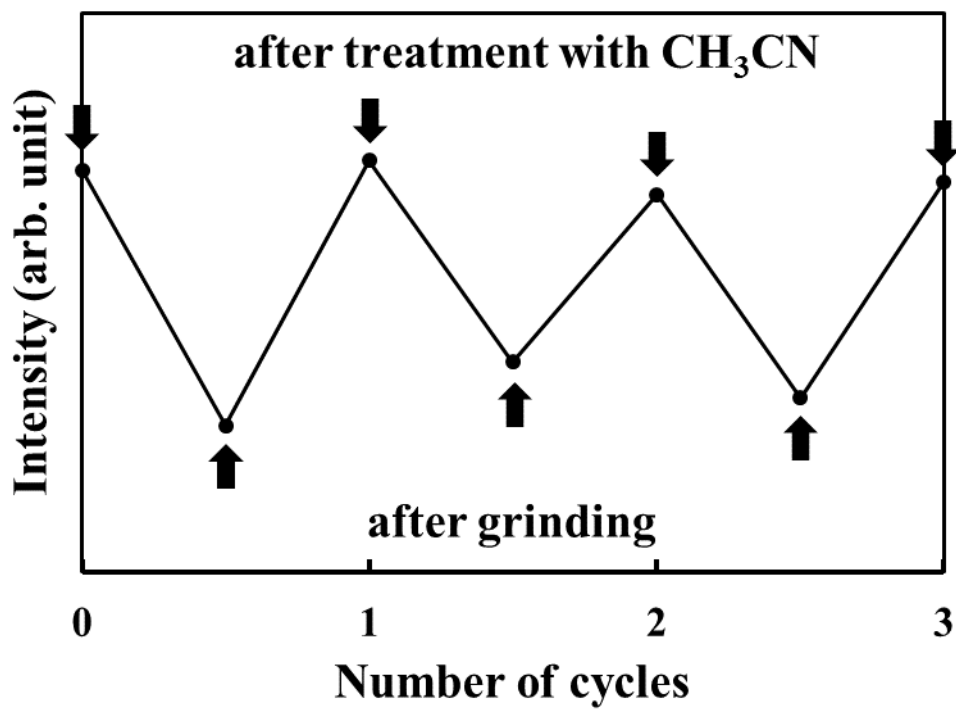


Fig. 15